J Chin Med Assoc

ORIGINAL ARTICLE

Deep learning-based workflow for automatic extraction of atria and epicardial adipose tissue on cardiac computed tomography in atrial fibrillation

Ling Kuo[a,b,c], Guan-Jie Wang[a], Po-Hsun Su[a], Shih-Ling Chang[b,c], Yenn-Jiang Lin[b,c], Fa-Po Chung[b,c], Li-Wei Lo[b,c], Yu-Feng Hu[b,c], Chin-Yu Lin[b,c], Ting-Yung Chang[b,c], Shih-Ann Chen[b,c,d,e,*], Chia-Feng Lu[a,*]

[a]Department of Biomedical Imaging and Radiological Sciences, National Yang Ming Chiao Tung University, Taipei, Taiwan, ROC; [b]Heart Rhythm Center, Division of Cardiology, Department of Medicine, Taipei Veterans General Hospital, Taipei, Taiwan, ROC; [c]Department of Internal Medicine, College of Medicine, National Yang Ming Chiao Tung University, Taipei, Taiwan, ROC; [d]Cardiovascular Center, Taichung Veterans General Hospital, Taichung, Taiwan, ROC; [e]College of Medicine, National Chung Hsing University, Taichung, Taiwan, ROC

Abstract

Background: Preoperative estimation of the volume of the left atrium (LA) and epicardial adipose tissue (EAT) on computed tomography (CT) images is associated with an increased risk of atrial fibrillation (AF) recurrence. We aimed to design a deep learning-based workflow to provide reliable automatic segmentation of the atria, pericardium, and EAT for future applications in the management of AF.

Methods: This study enrolled 157 patients with AF who underwent first-time catheter ablation between January 2015 and December 2017 at Taipei Veterans General Hospital. Three-dimensional (3D) U-Net models of the LA, right atrium (RA), and pericardium were used to develop a pipeline for total, LA-EAT, and RA-EAT automatic segmentation. We defined fat within the pericardium as tissue with attenuation between –190 and –30 HU and quantified the total EAT. Regions between the dilated endocardial boundaries and endocardial walls of the LA or RA within the pericardium were used to detect voxels attributed to fat, thus estimating LA-EAT and RA-EAT.

Results: The LA, RA, and pericardium segmentation models achieved Dice coefficients of 0.960 ± 0.010, 0.945 ± 0.013, and 0.967 ± 0.006, respectively. The 3D segmentation models correlated well with the ground truth for the LA, RA, and pericardium (r = 0.99 and $p < 0.001$ for all). The Dice coefficients of our proposed method for EAT, LA-EAT, and RA-EAT were 0.870 ± 0.027, 0.846 ± 0.057, and 0.841 ± 0.071, respectively.

Conclusion: Our proposed workflow for automatic LA, RA, and EAT segmentation using 3D U-Nets on CT images is reliable in patients with AF.

Keywords: Artificial intelligence; Atrial fibrillation; Epicardial adipose tissue; Machine learning

1. INTRODUCTION

Atrial fibrillation (AF) is the most common cardiac arrhythmia and can alter the morphology and function of the left atrium (LA) and epicardial adipose tissue (EAT).[1,2] Before AF treatment, pulmonary vein computed tomography (PVCT), a type of contrast-enhanced cardiac computed tomography (CT), is commonly used in performing safe and successful ablation procedures.[3] Cardiac CT is the gold standard technique for measuring atrial and EAT volumes because it can achieve high spatial resolution and whole-heart coverage.[4] Studies have demonstrated that the volumes of LA,[5–7] right atrial (RA),[8,9] total EAT,[10,11] and LA-EAT[11,12] measured on CT images are important predictors of AF recurrence following catheter ablation.

In clinical practice, cardiologists often perform manual delineation for atrial and EAT segmentation to estimate the volumes. However, manual segmentation is extremely time-consuming and subjective. Automatic segmentation of the atria and EAT in cardiac CT images using deep learning is valuable in improving its consistency and efficiency. Multiple studies have designed different network architectures to extract cardiac structures, including the LA, RA, left ventricle (LV), right ventricle (RV), and LV myocardium from cardiac CT data.[13–16] However, in these studies on whole-heart segmentation, the datasets used to develop the deep learning models were not aimed at a specific disease, such as AF. Additionally, because AF may lead to structural remodeling, including LA dilatation and tissue fibrosis,[1]

* *Address correspondence. Prof. Chia-Feng Lu, Department of Biomedical Imaging and Radiological Sciences, National Yang Ming Chiao Tung University, 155, Section 2, Linong Street, Taipei 112, Taiwan, ROC. E-mail address: alvin4016@nycu.edu.tw (C.-F. Lu); Dr. Shih-Ann Chen, Cardiovascular Center, Taichung Veterans General Hospital, 1650 Taiwan Boulevard Section 4, Taichung 407, Taiwan, ROC. E-mail address: epsachen@ms41.hinet.net (S.-A. Chen).*

Author contributions: Dr. Ling Kuo and Mr. Guan-Jie Wang contributed equally to this study.

Conflicts of interest: Dr. Shih-Ann Chen, an editorial board member at Journal of the Chinese Medical Association, had no role in the peer review process of or decision to publish this article. The other authors declare that they have no conflicts of interest related to the subject matter or materials discussed in this article.

Journal of Chinese Medical Association. (2024) 87: 471-479.

Received December 24, 2023; accepted February 4, 2024.

doi: 10.1097/JCMA.0000000000001076

reliable automatic segmentation of cardiac structures may not have been achieved in these deep learning models. Recent studies have developed deep-learning models for automatic LA segmentation in patients with AF.[17,18] However, in patients with AF, it would be valuable to develop a comprehensive segmentation system that includes the atria, pericardium, and EAT to predict AF recurrence following catheter ablation. No current studies have proposed a complete workflow for the automatic segmentation of cardiac structures associated with AF recurrence to provide a convenient system for clinical use. In total EAT segmentation, although some semi-automatic methods have been proposed to identify the Hounsfield units (HU) corresponding to fat, these methods still require manual delineation of the pericardium as the outer boundary, which does not prevent the time spent on contouring and interobserver variability.[19,20] Furthermore, studies have proposed the extraction of total EAT volume using deep learning algorithms in non-contrast or contrast-enhanced cardiac CT images; however, automatic segmentation of LA- and RA-EAT volumes has not yet been developed.[11,12,21–23]

In this study, we aimed to provide a new workflow for automatically segmenting the atria, pericardium, and EAT in contrast-enhanced cardiac CT images of patients with AF. Automatic segmentation in this system based on deep learning can achieve reliable results, improve efficiency, and contribute to future imaging studies on AF.

2. METHODS

2.1. Dataset for development of auto-segmentation models

We retrospectively collected contrast-enhanced cardiac CT images of 157 patients with AF from the Taipei Veterans General Hospital (TVGH). Cardiac CT was performed to assess the morphology of LA and pulmonary veins before catheter ablation. The inclusion criteria were as follows: (1) sufficient image quality for the evaluation of the LA and pulmonary veins; (2) no metal implants in the cardiac chambers; and (3) the presence of the whole heart within the image volume. This study was approved by the Institutional Review Board of TVGH (VGH-IRB Number: 2022-06-016AC) and the requirement for informed consent was waived.

2.2. Cardiac CT acquisition

Cardiac CT scans were acquired using 64-slice (Aquilion 64, Toshiba Medical Systems) and 256-slice (Brilliance iCT, Philips Healthcare) scanners. The Aquilion 64 used a peak tube voltage of 100 kVp and a tube current of 350 mA, whereas the Brilliance iCT used a peak tube voltage of 100 or 120 kVp and a tube current of 596 mA. The 16-bit and 12-bit grayscale PVCT images were generated using the Aquilion 64 and Brilliance iCT, respectively. Cardiac CT images from each patient were reconstructed using a slice thickness of 1 mm and stored in the Digital Imaging and Communications in Medicine (DICOM) format with a matrix size of 512×512. The variation in pixel sizes for the reconstructed images was 0.34×0.34 to $0.72 \times 0.72\,mm^2$.

2.3. Manual labeling

The LA, RA, and pericardium were manually contoured using the Multimodal Radiomics Platform (http://cflu.lab.nycu.edu.tw/MRP_MLinglioma.html), which was developed in the MATLAB environment.[24] Cardiac CT images viewed on this platform were displayed with a soft tissue window (window center: 40 HU, window width: 400 HU) to improve the contrast of all cardiac structures. Regions of interest (ROIs) for the LA and RA, including the atrial appendages, were contoured by tracing the atrial endocardial boundaries. The upper border of the pericardium was defined as the top slice of the LA, whereas the inferior border was defined as the last slice containing any part of the cardiac chambers.[25] All ROIs were delineated by experienced radiologic technologists and cardiologists.

2.4. Image preprocessing

Full-range cardiac CT and ROI images were preprocessed. First, the adjustments of the image resolution were resampled into the isotropic voxels of $0.5 \times 0.5 \times 0.5\,mm^3$. Second, the z-direction of all the images was adjusted to the same slice size. On the cardiac CT images, the aortic arch was identified as the initial slice and included the next caudal 320 slices to encompass the entire heart. If a patient had a large cardiac morphology, the initial slice was moved down until the entire heart was covered. Third, the images were cropped to 400×400 pixels to ensure that the ROIs of the LA, RA, and pericardium were included in the matrix. The CT images were further normalized to the soft tissue window and subsequently rescaled to 8-bit grayscale from 0 to 255. Finally, the matrix size of the CT and ROI images was $400 \times 400 \times 320$ with isotropic voxels of $0.5 \times 0.5 \times 0.5\,mm^3$. The input size of the three-dimensional (3D) U-Net was further downsampled to $200 \times 200 \times 160$ with an interpolation of the voxel size to $1 \times 1 \times 1\,mm^3$. All image preprocessing steps were performed using MATLAB 2020a.

2.5. Deep learning models

Hundreds of labeled images were prepared to create a training set for 3D segmentation. However, manual delineation of the LA, RA, and pericardium in all patients with AF in the dataset was laborious. Hence, we used two-dimensional (2D) U-Nets trained on 30 patients, which included 9600 images, to assist with manual labeling. The architecture and training parameters of the 2D U-Nets are presented in the Supplementary Materials, http://links.lww.com/JCMA/A238. The results of the 2D U-Net segmentation for the LA, RA, and pericardium were modified by erasing or filling incorrect regions. For 3D segmentation, the dataset consisted of 157 patients divided into training and testing sets of 125 and 32 patients, respectively. To improve the predictive ability, data augmentation was applied to increase the size and variability of the training set.[26] The training images were rotated by 10°, 20°, and –20°, thus resulting in 500 image volumes that were used as the new training set.

Our proposed 3D U-Net architecture consists of 22 convolutional layers with concatenation between the encoders and decoders. The encoders consist of repeated applications of three convolutional layers with $3 \times 3 \times 3$ kernels, each followed by batch normalization and ReLU processes. After every three convolutions, $2 \times 2 \times 2$ max-pooling with a stride of 2 was applied in succession. Each decoder consisted of a $2 \times 2 \times 2$-transposed convolutional kernel with a stride of 2 and three $3 \times 3 \times 3$ convolutional layers followed by batch normalization and ReLU. Finally, a $1 \times 1 \times 1$ convolutional layer with a softmax function was used to predict the probability of each pixel. The proposed 3D U-Net architecture is illustrated in Fig. 1.

The experimental environment was implemented using MATLAB 2020a with 6 GB NVIDIA GeForce RTX 2060 GPU, Intel Core i7-9700 CPU, and 40 GB of RAM. The training model used a stochastic gradient descent with a momentum of 0.9 to update the weight of the network. The training parameters for the 3D U-Net models were as follows: learning rate = 0.01, mini-batch size = 2, maximum epoch = 32, learning rate drop period = 10, and learning rate drop factor = 0.3. The dice loss was used as the loss function. It took approximately 52 hours and 50 minutes to complete the training of the models for the LA, RA, and pericardium segmentation, respectively.

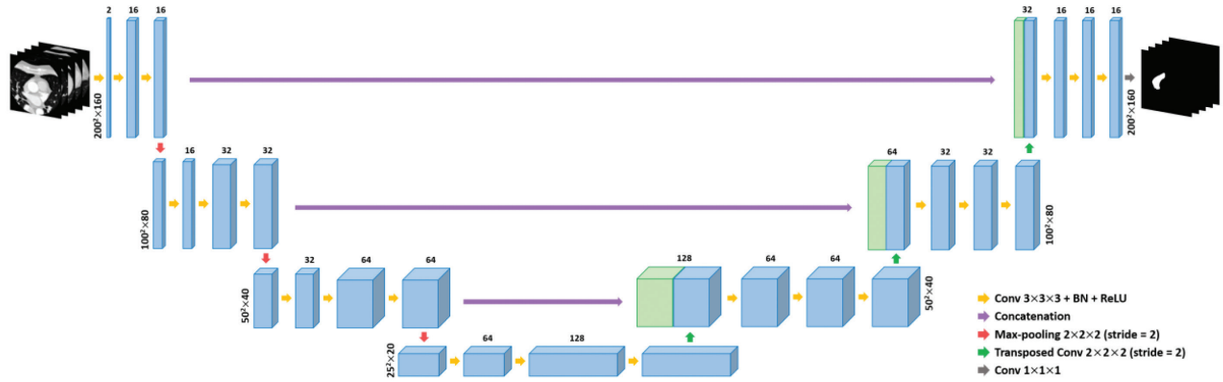

Fig. 1 3D U-Net architecture. U-Net is the most famous fully convolutional neural network for satisfactory biomedical image segmentation. Three independent 3D U-Net models for LA, RA, and pericardium segmentation were developed. 3D = three-dimensional; LA = left atrium; RA = right atrium.

2.6. EAT segmentation

EAT is the visceral fat deposited between the myocardium and the pericardium.[27] After automatically segmenting the pericardium using 3D U-Net (Fig. 2A), cardiac CT images were resampled to the original voxel size of $0.5 \times 0.5 \times 0.5\,mm^3$, and the voxels corresponding to EAT were identified. Cardiac CT included contrast injection; therefore, a higher HU of −190 to −30 was used to identify the voxels within the pericardium.[28,29] The sum of all the detected voxels within the pericardium was defined as the total EAT (Fig. 2B).

LA-EAT and RA-EAT represent the fat accumulated around the LA and RA, respectively. The LA and RA contours were extracted from the LA and RA ROIs segmented using the proposed 3D U-Nets (Fig. 2C). Previously, Wang et al[30] found that the mean thickness of the left and right atrioventricular groove EAT was 12.7 and 13.9 mm, respectively. Based on this evidence, the endocardial boundaries of the LA and RA were individually dilated by 15 mm to identify the fat surrounding the atria.

The areas for identifying the voxels of the LA-EAT and RA-EAT were between the endocardial wall and the dilated boundaries (Fig. 2D). We automatically segmented the ROIs within the pericardium to exclude the extrapericardial fat (Fig. 2A). Pixels between −190 and −30 HU were found at the intersection of the dilated regions and pericardium ROIs (Fig. 2E). Some pixels were a part of both LA-EAT and RA-EAT; therefore, all pixels were reassigned. The minimum Euclidean distance was applied to measure the distance between each EAT pixel and both atria as follows:

$$d = \sqrt{(x_1 - x_2)^2 + (y_1 - y_2)^2},$$

where d is the minimum distance, and the coordinates of the EAT pixel and the pixel situated at the atrial endocardial boundary are (x_1, y_1) and (x_2, y_2), respectively. When the minimum Euclidean distance of a pixel as an EAT from the LA was shorter than the distance from the RA, the pixel was considered LA-EAT and vice versa (Fig. 2F). When the minimum distance of an EAT pixel from the LA was equal to the distance from the RA, the EAT pixel was considered shared by LA-EAT and RA-EAT.

2.7. Assessment of model performance

To compare the similarity between manual and automatic segmentation, we used the Dice coefficient, sensitivity, and precision as statistical metrics,[31] which are defined as follows:

$$\text{Dice}\,(A, B) = \frac{2\ |A \cap B|}{|A| + |B|}$$

where A is automatic segmentation and B is manual segmentation. The Dice coefficient is between 0 and 1, with 0 indicating no segmentation overlap and 1 indicating perfect segmentation overlap.

$$\text{Sensitivity} = \frac{\text{TP}}{\text{TP} + \text{FN}}$$

$$\text{Precision} = \frac{\text{TP}}{\text{TP} + \text{FP}}$$

Overlapping pixels are classified into four categories: true positive (TP), true negative (TN), false positive (FP), and false negative (FN).

We further measured the percentage volume difference (PVD) to compare the differences between manual and automatic segmentation based on the following formula:

$$\text{PVD} = \frac{V_A - V_B}{\frac{1}{2}(V_A + V_B)} \times 100\%,$$

where V_A is the volume of automatic segmentation and V_B is the volume of manual segmentation. Volume measurements were performed by multiplying the voxel size by the sum of the voxels corresponding to each label.

2.8. Statistical analysis

Continuous variables, including the Dice coefficient, sensitivity, precision, and volume difference, are stated as mean ± SD. The volume difference between automatic and manual segmentation was assessed using a single-tailed paired t test. Bland-Altman plots and Pearson correlation coefficients were used to estimate the bias and levels of agreement between automatic and manual segmentation. Statistical significance for all comparisons was set at $p < 0.05$. The statistical analyses were performed using MATLAB 2020a.

3. RESULTS

3.1. Performance of auto-segmentation for LA, RA, and pericardium

This dataset included 157 patients with AF. Baseline characteristics and CT measurements are shown in Table 1. There were no

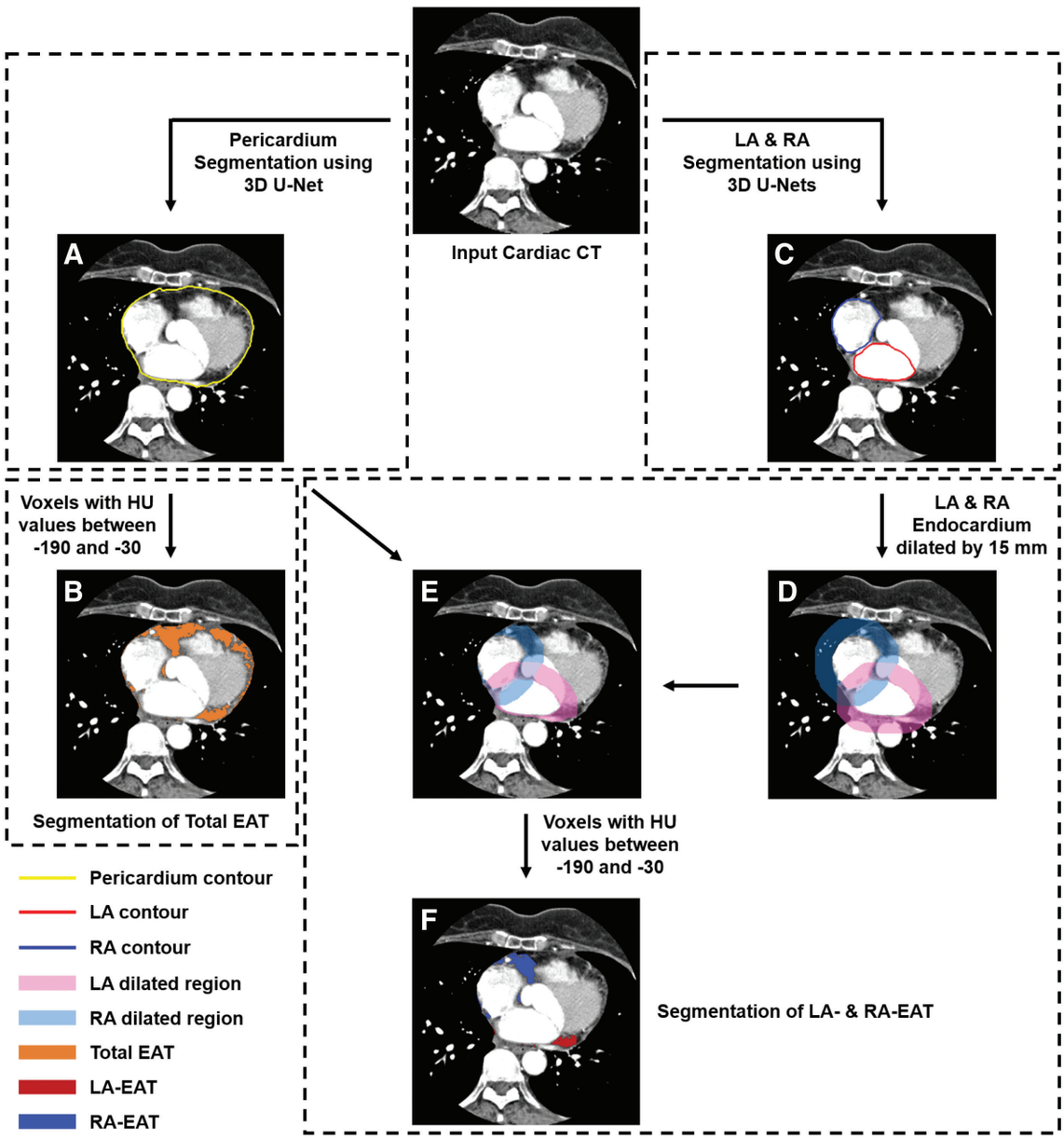

Fig. 2 Flowchart of total EAT, LA-EAT, and RA-EAT segmentation. A, The results of 3D pericardium segmentation. B, The results of total EAT segmentation within the pericardium, which identifies voxels with HU values between –190 and –30. C, The results of 3D LA and RA segmentation. Combining the steps of D–F yielded the results of LA- and RA-EAT segmentation. 3D = three-dimensional; EAT = epicardial adipose tissue; HU = Hounsfield unit; LA = left atrium; RA = right atrium.

significant differences in patient comorbidities, left ventricular systolic function, or volumes of the atria, and EAT in training and testing datasets. Comparisons and evaluation metrics of the ground truth and automatic segmentation using 2D U-Net assistance are presented in Supplementary Figs. S1 and S2, http://links.lww.com/JCMA/A238. With the assistance of 2D U-Net, doctors can obtain initial 3D contours of the LA, RA, and pericardium to further apply manual revisions, especially around the pulmonary vein-LA junction, RA-superior vena cava junction, RA-inferior vena cava junction, and pericardium of the inferior ventricle.

The final 3D U-Net segmentation for the LA, RA, and pericardium required approximately 7.42 seconds per patient. For 3D U-Net models, the resultant LA, RA, and pericardium segmentation achieved Dice coefficients of 0.960 ± 0.010, 0.945 ± 0.013, and 0.967 ± 0.006, respectively. The sensitivity obtained using 3D U-Net models of LA, RA, and pericardium was 0.946 ± 0.023, 0.938 ± 0.026, and 0.965 ± 0.014, whereas the precision was 0.974 ± 0.013, 0.954 ± 0.024, and 0.969 ± 0.010, respectively. Supplementary Fig. S3, http://links.lww.com/JCMA/A238, presents the box plots of the Dice coefficients, sensitivity, and precision for the LA, RA, and pericardium using the testing dataset of 32 patients. Fig. 3 presents a visual assessment of the 3D segmentation of the LA, RA, and pericardium.

The agreement and correlation between the cardiac volumes obtained using 3D U-Net and manual segmentation are shown

Table 1

Baseline characteristics and computed tomography measurements

Variables	Total (n = 157)	Training (n = 125)	Testing (n = 32)	*p*
Age, y	55.3 ± 10.0	55.0 ± 10.3	56.3 ± 8.9	0.5
Male, %	127 (80.9)	101 (80.8)	26 (81.3)	1
Body height, cm	169.5 ± 7.7	169.4 ± 7.6	170.0 ± 8.2	0.7
Body weight, kg	73.5 ± 12.3	72.8 ± 11.5	76.0 ± 14.8	0.2
Body mass index, kg/m²	25.4 ± 3.8	25.1 ± 3.6	26.2 ± 4.5	0.1
Body surface area, m²	1.9 ± 0.2	1.85 ± 0.2	1.89 ± 0.2	0.3
Hypertension, n (%)	71 (45.2)	52 (41.6)	19 (59.4)	0.08
Diabetes mellitus, n (%)	15 (9.6)	11 (8.8)	4 (12.5)	0.5
Ischemic stroke, n (%)	9 (5.7)	5 (4.0)	5 (12.5)	0.09
hyperlipidemia, n (%)	24 (15.3)	20 (16.0)	4 (12.5)	0.8
Non-paroxysmal atrial fibrillation, n (%)	66 (42)	52 (41.6)	14 (43.8)	0.8
LVEF, %	57.4 ± 6.4	57.8 ± 6.0	56.1 ± 7.7	0.2
Left atrial volume, mL	126.7 ± 34.9	124.4 ± 35.1	135.2 ± 33.1	0.1
Right atrial volume, mL	122.7 ± 44.5	121.1 ± 46.9	128.7 ± 33.9	0.4
Left atrial EAT volume, mL	15.7 ± 6.7	15.7 ± 6.9	15.9 ± 6.0	0.9
Right atrial EAT volume, mL	21.6 ± 7.7	21.2 ± 7.5	23.4 ± 8.6	0.1

Values are mean ± SD or n (%).

EAT = epicardial adipose tissue; LVEF = left ventricular ejection fraction.

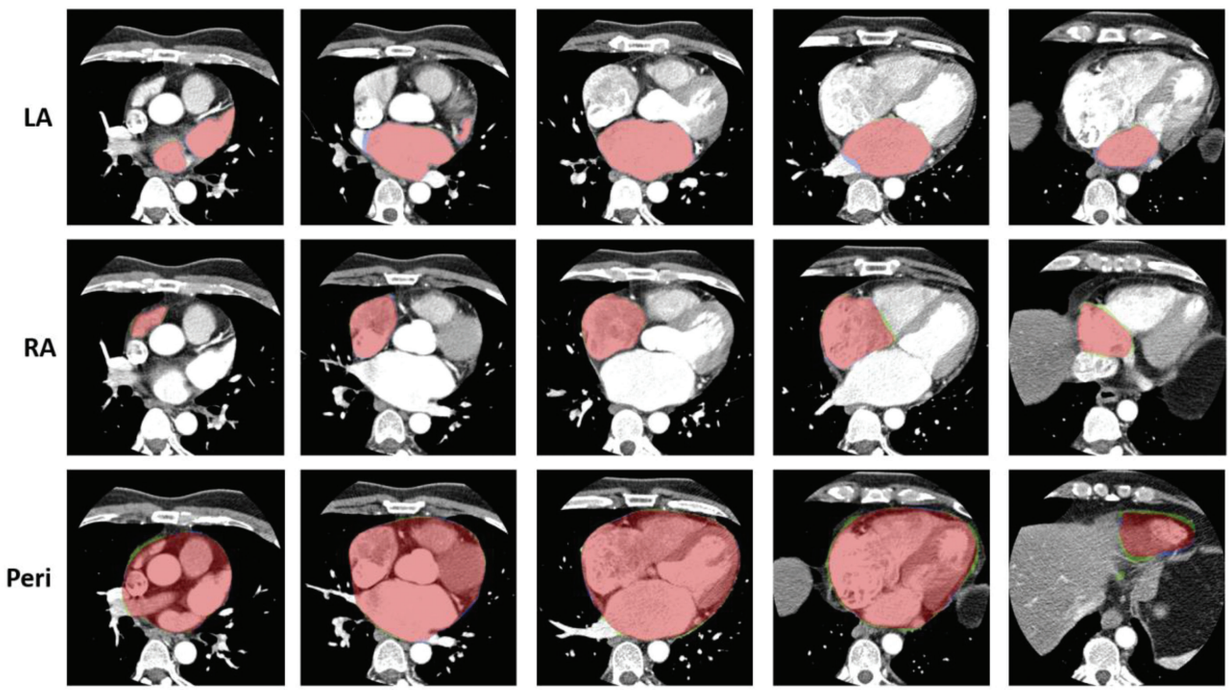

Fig. 3 Ground truth and 3D U-Net segmentation of LA, RA, and pericardium. The blue and green colors represent the ground truth and automatic segmentation of 3D U-Nets. The red color is the overlapping regions of ground truth and the automatic segmentation. 3D = three-dimensional; LA = left atrium; Peri = pericardium; RA = right atrium.

in Fig. 4. The volumes of LA, RA, and pericardium calculated by manual and automatic segmentation were 139.5 ± 33.2 vs 135.5 ± 32.6 mL, 131.4 ± 34.0 vs 129.1 ± 33.9 mL, and 899.0 ± 134.9 vs 895.3 ± 139.0 mL, respectively. Pearson correlation analysis revealed that manual and automatic segmentation had a significantly high correlation for all cardiac structures (r = 0.99 for LA, RA, and pericardium, p < 0.001). Bland-Altman plots revealed a volume difference of −4.01 ± 4.62, −2.34 ± 5.85, and −3.73 ± 18.80 mL, and PVD of −3.07 ± 3.35%, −1.89 ± 4.63%, and −0.50 ± 2.24%, respectively. The volumes of the LA (p < 0.001) and RA (p = 0.016) segmented using 3D U-Nets were significantly smaller than those segmented manually. For the segmentation of the pericardium, there was no significant volume difference between manual and automatic segmentation (p = 0.135).

3.2. Performance of auto-segmentation for EAT segmentation

The volumes of total EAT, LA-EAT, and RA-EAT calculated using manual and automatic segmentation were 91.3 ± 37.7

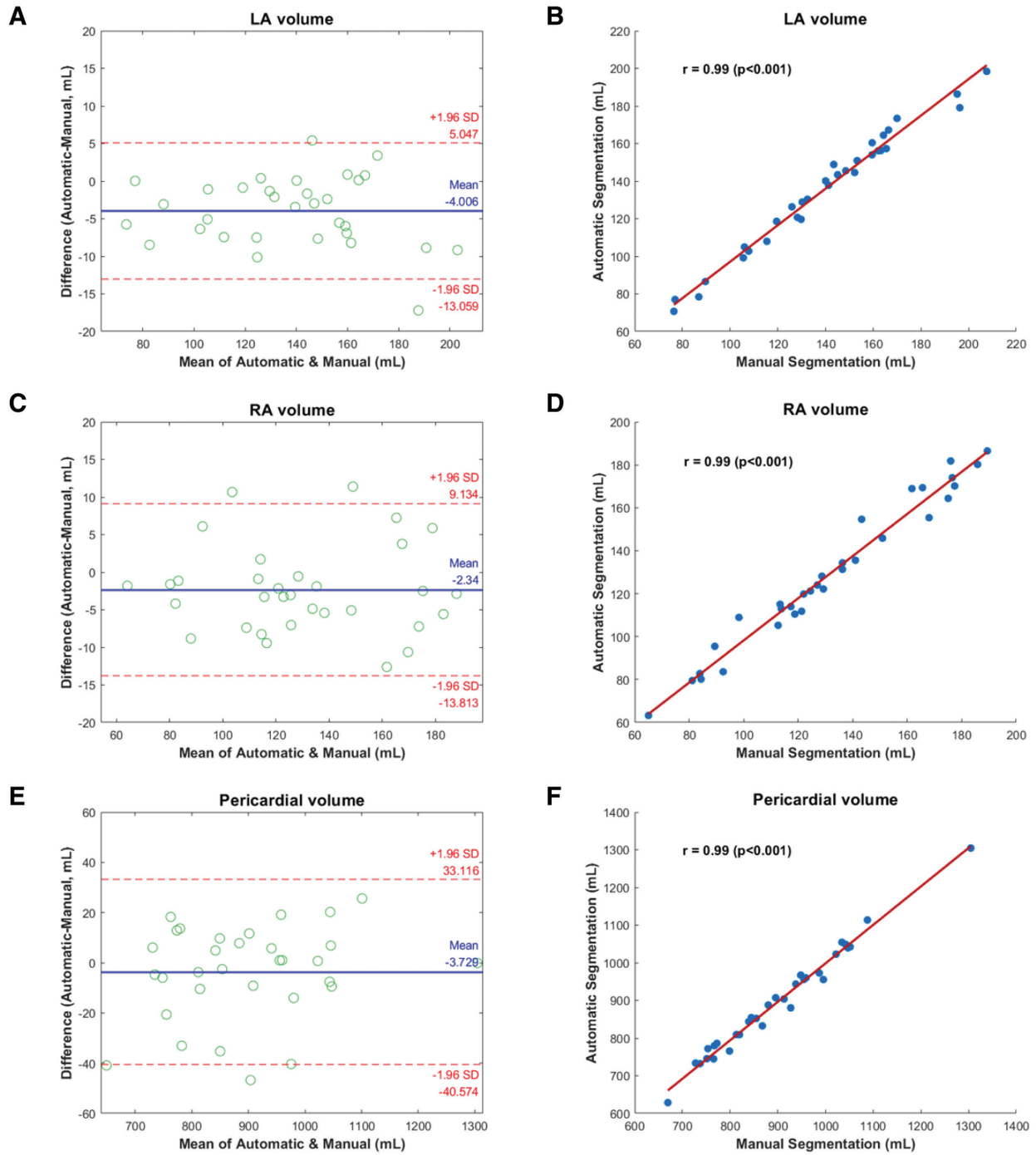

Fig. 4 Comparison of the agreement for 3D automatic segmentation with manual segmentation of LA, RA, and pericardium volumes. Bland-Altman analysis between our proposed 3D segmentation models and ground truth for LA (A), RA (C), and pericardium (E) volumes show mean bias (95% limits of agreement) of –4.01 (–13.06, 5.05) mL, –2.34 (–13.81, 9.13) mL, and –3.73 (–40.57, 33.12) mL, respectively. Excellent correlations are found in 3D U-Net models against ground truth for LA (B), RA (D), and pericardium (F), all indicating $r = 0.99$ ($p < 0.001$). In Bland-Altman plots, blue line indicates the mean difference and the two red dashed lines indicate the limits of agreement, from –1.96 to +1.96 SDs. 3D = three-dimensional; EAT = epicardial adipose tissue; LA = left atrium; RA = right atrium.

vs 93.8 ± 35.8 mL, 16.0 ± 5.9 vs 16.0 ± 6.0 mL, and 24.9 ± 14.3 vs 23.8 ± 8.8 mL, respectively. Pearson correlation analysis revealed that the volumes estimated using manual and automatic segmentation revealed a significantly high correlation with EAT quantification (r = 0.98, 0.97, and 0.93 for total EAT, LA-EAT, and RA-EAT, respectively; $p < 0.001$). The performance of total EAT segmentation within pericardial regions revealed a Dice coefficient of 0.870 ± 0.027, sensitivity of 0.888 ± 0.033, and precision of 0.856 ± 0.052. Our proposed method yielded a Dice coefficient of 0.846 ± 0.057, sensitivity

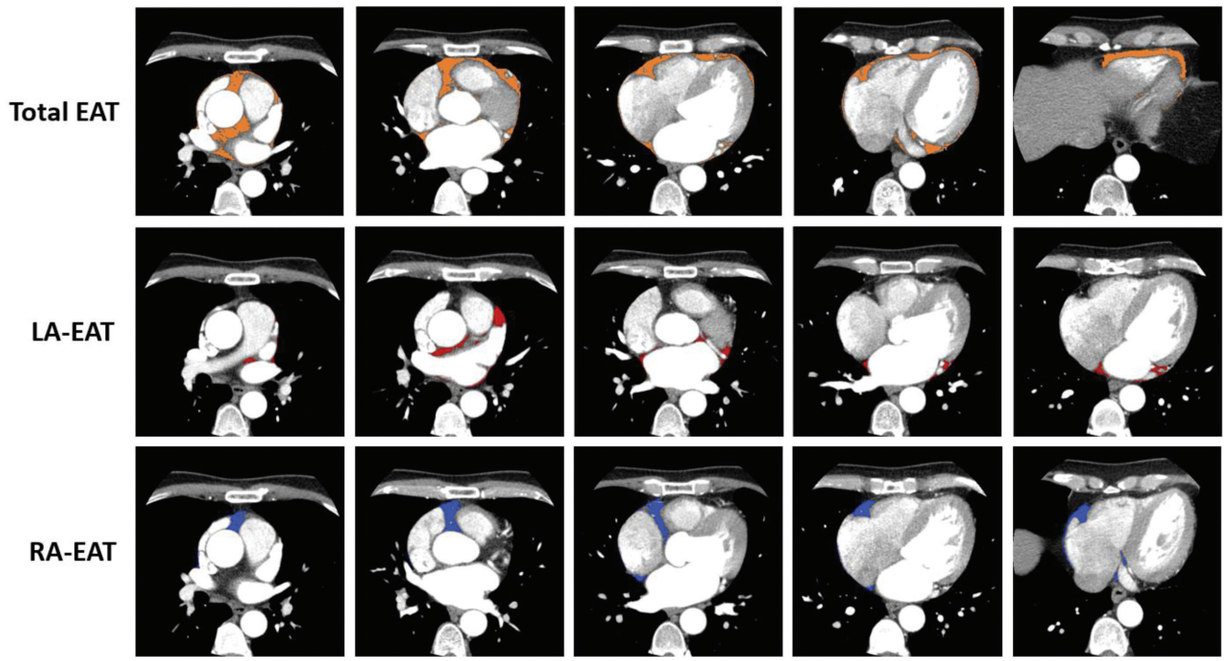

Fig. 5 Distribution of total EAT, LA-EAT, and RA-EAT in different CT axial slices. The brown, red, and blue regions represent the total EAT, LA-EAT, and RA-EAT identifying HU values between –190 and –30, respectively. EAT = epicardial adipose tissue; LA = left atrium; RA = right atrium.

of 0.861 ± 0.051, and precision of 0.836 ± 0.082 for LA-EAT segmentation, and a Dice coefficient of 0.841 ± 0.071, sensitivity of 0.839 ± 0.070, and precision of 0.846 ± 0.085 for RA-EAT segmentation. EAT segmentation, including total EAT, LA-EAT, and RA-EAT took approximately 31.35 seconds per patient. LA-EAT was concentrated primarily in three regions: (a) areas surrounded by the ascending aorta, right superior pulmonary vein, and superior vena cava; (b) areas between the left atrial appendage and the pulmonary trunk; and (c) areas within the left atrioventricular groove. RA-EAT was primarily concentrated in the right atrioventricular groove. A small part of the RA-EAT was located in areas posterior to the RA and between the RA and the coronary sinus. The results of automatic segmentation for total EAT, LA-EAT, and RA-EAT are presented in Fig. 5.

4. DISCUSSION

In this study, we proposed a full workflow based on deep learning to provide reliable and rapid automatic segmentation of the atria, pericardium, and EAT on contrast-enhanced cardiac CT images in patients with AF. In clinical practice, an experienced cardiologist would need to spend approximately 3 hours manually delineating the atria and the total EAT. In this study, we only required approximately 30 seconds to obtain the volumes of LA, RA, pericardium, and EAT, which included the total EAT, LA-EAT, and RA-EAT, in patients with AF. Therefore, this workflow provides time-efficient automatic segmentation to facilitate the prediction of AF recurrence.

We have summarized the methods and performances of our proposed models and the following articles on cardiac and EAT segmentation in Table 2. The LA volume measured on preoperative contrast-enhanced CT scans is an important predictor of AF recurrence[5–7]; therefore, some studies have developed LA segmentation using deep learning on CT images in patients with AF. Two studies used a pipeline of two 2D convolutional neural networks (CNN) in patients with AF—the first CNN was designed for LA detection and the second CNN was designed for LA segmentation.[17,18] Chen et al[17] achieved an intersection over union of 0.914, while Abdulkareem et al[18] achieved a Dice coefficient of 0.885 ± 0.12. Compared with studies that used the 2D approaches described above, the present study achieved superior performance in LA segmentation (Dice coefficient = 0.960 ± 0.010) because 3D segmentation provides global contextual information from volumetric CT images, which can particularly assist in separating the boundaries of the LA and pulmonary veins. Additionally, our proposed workflow could provide segmentation of other significant AF recurrence predictors, such as RA,[8,9] total EAT,[10,11] and LA-EAT,[11,12] which aids in comprehensive assessments of patients with AF undergoing catheter ablation.

Several studies have presented whole-heart segmentation using 3D deep learning methods, including the segmentation of the LA, RA, LV, RV, and LV myocardium. The LA and RA segmentations in these studies achieved Dice coefficients of 0.889 to 0.939 and 0.812 to 0.878, respectively.[13,14,16] We used a dataset of more CT scans with sufficient variability in cardiac morphology; therefore, we achieved superior performance in LA and RA segmentation (LA: 0.960 ± 0.010; RA: 0.945 ± 0.013) compared with these studies. To make the segmentation models practical and meaningful, we also evaluated the volume difference and the correlation between manual and automatic segmentation results. Although the LA and RA volumes of our proposed 3D segmentation were significantly smaller than those of manual segmentation, the PVD of the LA and RA were in the clinically acceptable range of 2% to 3%. Baskaran et al[15] used 2D U-Net and obtained a great correlation in RA segmentation (r = 0.97), but a slightly lower correlation in LA segmentation (r = 0.78). This may be because it was difficult to segment the blurred junctions between the contrast-filled LA and LV using 2D segmentation. In contrast, our 3D models provided complete contextual information and achieved high correlation coefficients in LA (r = 0.99)

Table 2

Related publications on cardiac CT and EAT segmentation using deep learning

Publications	Networks	Imaging types	Dataset	Segmentation targets	Structures and testing results
Chen et al[17]	A pipeline of ResNet50/U-Net (2D)	CECT	97 paroxysmal AF patients	LA	Mean IoU = 0.914
Abdulkareem et al[18]	A pipeline of ResNet50/U-Net (2D)	CECT	150 AF patients	LA	DSC = 0.885 ± 0.12
Tong et al[14]	Deeply supervised U-Net (3D)	CECT/MRI	60 CT and 60 MRI scans from multiple cardiac diseases	LA, RA, LV, RV, LVM	Mean DSC: LA = 0.889; RA = 0.812; LV = 0.893; RV = 0.810; LVM = 0.837
Payer et al[15]	A pipeline of two FCNs (3D)	CECT/MRI	60 CT and 60 MRI scans from multiple cardiac diseases	LA, RA, LV, RV, LVM	Mean DSC: LA = 0.924; RA = 0.878; LV = 0.924; RV = 0.879; LVM = 0.872
Sharobeem et al[16]	A pipeline of SqueezeNet/dense V-Net (3D)	CECT	71 patients undergoing TVAI	LA, RA, LV, RV, LVM	Median DSC: LA = 0.939; RA = 0.877; LV = 0.852; RV = 0.819; LVM = 0.927
Baskaran et al[15]	U-Net (2D)	CECT	166 asymptomatic subjects with no CAD	LA, RA, LV, RV, LVM	Median DSC: LA = 0.934; RA = 0.915; LV = 0.938; RV = 0.927; LVM = 0.920
Commandeur et al[32]	ConvNets (2.5D)	NCCT	850 scans from asymptomatic subjects with no CAD	Total EAT	Median DSC = 0.873
Hoori et al[22]	DeepLab-v3-plus (2.5 D)	NCCT	89 healthy subjects	Total EAT	DSC = 0.8852 ± 0.033
He et al[33]	Deep attention U-Net (3D)	CECT	200 patients with CAD	Total EAT	DSC = 0.887 ± 0.068
Present study	U-Net (3D)	CECT	157 patients with AF	LA, RA, pericardium, total EAT, LA-EAT, RA-EAT	DSC: LA = 0.960 ± 0.010; RA = 0.945 ± 0.013; Pericardium = 0.967 ± 0.006; Total EAT = 0.870 ± 0.027; LA-EAT = 0.846 ± 0.057; RA-EAT = 0.841 ± 0.071

AF = atrial fibrillation; CAD = coronary artery disease; CECT = contrast-enhanced computed tomography; CT = computed tomography; DSC = Dice score; EAT = epicardial adipose tissue; FCN = fully convolutional neural network; IoU = intersection over union; LA = left atrium; LV = left ventricle; LVM = left ventricular myocardium; MRI = magnetic resonance imaging; NCCT = non-contrast computed tomography; RA = right atrium; RV = right ventricle.

and RA (r = 0.99) segmentation. Hence, the 3D U-Net with volumetric data input outperforms the 2D U-Net with single-slice input in segmenting the complex structures of the heart.

In the present study, contrast-enhanced cardiac CT images were used to perform pericardial and total EAT segmentation. The major advantage of contrast-enhanced CT is that it is easier to detect the pericardium than using non-contrast CT images. Although Commandeur et al[32] included 850 non-contrast CT scans from multiple cohorts to develop a fully automatic approach for total EAT segmentation, they obtained a result (median Dice = 0.873) comparable to that of the present study (median Dice = 0.874), which included 157 contrast-enhanced CT scans. Therefore, a large dataset is required for the model to learn automatic segmentation of the total EAT within the pericardium using non-contrast CT images. Additionally, although Hoori et al[22] used transfer learning with a bisect method to segment the total EAT within the pericardium using non-contrast CT images with a Dice coefficient of 0.8852 ± 0.033, the total EAT segmentation in the present study using contrast-enhanced CT images only required a simple 3D U-Net. In another previous study, the total EAT segmentation proposed by He et al[33] used contrast-enhanced CT to develop a 3D deep attention U-Net and obtained a mean Dice coefficient (0.887) similar to that in our study (0.870). However, the present study had a smaller SD (0.027) of the Dice coefficient than that proposed by He et al[33] (SD of 0.068), thus indicating the superiority of our method.

In this study, we first proposed automatic segmentation of LA-EAT and RA-EAT by combining 3D U-Nets of the LA, RA, and pericardium. The Dice coefficients for LA-EAT and RA-EAT (0.84 and 0.95, respectively) were slightly lower than those for the LA, RA, and pericardium. The primary reason was that, according to our designed workflow, the performance of LA-EAT and RA-EAT depended on the accuracy of LA and pericardium segmentation as well as RA and pericardium segmentation, respectively. We believe that the automatic segmentation of LA-EAT and RA-EAT could be of help in future studies on AF in avoiding time-consuming and observer-dependent manual labeling and segmentation.

This study has several limitations. First, cardiac CT images were collected only from a single center that used CT scanners from two manufacturers. This indicates that the degree of data heterogeneity must increase. In the future, we will use images obtained using CT scans from multiple centers and different types of CT scanners to improve the adaptability of our deep learning models. Second, the manual delineation of all cardiac structures was based on consensus annotation from two experts, and interobserver variability was not assessed to validate the manual segmentation results. However, the contours of the atria and pericardium generated by manual delineation and 3D U-Net models were confirmed and could not be differentiated by a blinded expert physician (C.M. Liu). Third, this study included patients with AF and not normal volunteers or patients with other cardiovascular diseases. Contrast-enhanced cardiac CT images from patients with other heart diseases, such as dilated cardiomyopathy or myxoma, result in poor segmentation with 3D U-Net models. After labeling new data from other heart diseases, transfer learning can be used to fine-tune the neural networks to improve their use.

In conclusion, this study proposes a workflow for automatic segmentation of the LA, RA, pericardium, and EAT using deep learning using cardiac CT images of patients with AF. Furthermore, we developed automatic segmentation of LA-EAT and RA-EAT to prevent time-consuming manual delineation. In clinical practice, this workflow can assist in improving work efficiency and facilitate the prediction of AF recurrence.

ACKNOWLEDGMENTS

This study was supported by the grant of Taipei Veterans General Hospital (V112B-002), Szu-Yuan Research Foundation of Internal Medicine (113007), National Science and Technology Council (NSTC 112-2314-B-A49-060), Veterans General Hospitals and University System of Taiwan Joint Research Program (VGHUST113-G1-2-3).

APPENDIX A. SUPPLEMENTARY DATA

Supplementary data related to this article can be found at http://links.lww.com/JCMA/A238.

REFERENCES

1. Wijesurendra RS, Casadei B. Mechanisms of atrial fibrillation. *Heart* 2019;105:1860–7.
2. Conte M, Petraglia L, Cabaro S, Valerio V, Poggio P, Pilato E, et al. Epicardial adipose tissue and cardiac arrhythmias: focus on atrial fibrillation. *Front Cardiovasc Med* 2022;9:932262.
3. Di Cori A, Zucchelli G, Faggioni L, Segreti L, De Lucia R, Barletta V, et al. Role of pre-procedural CT imaging on catheter ablation in patients with atrial fibrillation: procedural outcomes and radiological exposure. *J Interv Card Electrophysiol* 2021;60:477–84.
4. Sarin S, Wenger C, Marwaha A, Qureshi A, Go BD, Woomert CA, et al. Clinical significance of epicardial fat measured using cardiac multislice computed tomography. *Am J Cardiol* 2008;102:767–71.
5. Shin SH, Park MY, Oh WJ, Hong SJ, Pak HN, Song WH, et al. Left atrial volume is a predictor of atrial fibrillation recurrence after catheter ablation. *J Am Soc Echocardiogr* 2008;21:697–702.
6. Costa FM, Ferreira AM, Oliveira S, Santos PG, Durazzo A, Carmo P, et al. Left atrial volume is more important than the type of atrial fibrillation in predicting the long-term success of catheter ablation. *Int J Cardiol* 2015;184:56–61.
7. Njoku A, Kannabhiran M, Arora R, Reddy P, Gopinathannair R, Lakkireddy D, et al. Left atrial volume predicts atrial fibrillation recurrence after radiofrequency ablation: a meta-analysis. *Europace* 2018;20:33–42.
8. Akutsu Y, Kaneko K, Kodama Y, Suyama J, Li HL, Hamazaki Y, et al. Association between left and right atrial remodeling with atrial fibrillation recurrence after pulmonary vein catheter ablation in patients with paroxysmal atrial fibrillation: a pilot study. *Circ Cardiovasc Imaging* 2011;4:524–31.
9. Takagi T, Nakamura K, Asami M, Toyoda Y, Enomoto Y, Moroi M, et al. Impact of right atrial structural remodeling on recurrence after ablation for atrial fibrillation. *J Arrhythm* 2021;37:597–606.
10. Stojanovska J, Kazerooni EA, Sinno M, Gross BH, Watcharotone K, Patel S, et al. Increased epicardial fat is independently associated with the presence and chronicity of atrial fibrillation and radiofrequency ablation outcome. *Eur Radiol* 2015;25:2298–309.
11. Nagashima K, Okumura Y, Watanabe I, Nakai T, Ohkubo K, Kofune T, et al. Association between epicardial adipose tissue volumes on 3-dimensional reconstructed CT images and recurrence of atrial fibrillation after catheter ablation. *Circ J* 2011;75:2559–65.
12. Tsao HM, Hu WC, Wu MH, Tai CT, Lin YJ, Chang SL, et al. Quantitative analysis of quantity and distribution of epicardial adipose tissue surrounding the left atrium in patients with atrial fibrillation and effect of recurrence after ablation. *Am J Cardiol* 2011;107:1498–503.
13. Tong Q, Ning M, Si W, Liao X, Qin J: 3D deeply-supervised U-net based whole heart segmentation. In: Mihaela Pop, Maxime Sermesant, Pierre-Marc Jodoin, Alain Lalande, Xiahai Zhuang, Guang Yang, Alistair Young, Olivier Bernard, editors. *Statistical Atlases and Computational Models of the Heart. ACDC and MMWHS Challenges*. Cham, Switzerland: Springer Cham; 2018, p. 224–32.
14. Payer C, Štern D, Bischof H, Urschler M: Multi-label whole heart segmentation using CNNs and anatomical label configurations. In: Mihaela Pop, Maxime Sermesant, Pierre-Marc Jodoin, Alain Lalande, Xiahai Zhuang, Guang Yang, Alistair Young, Olivier Bernard, editors. *Statistical Atlases and Computational Models of the Heart. ACDC and MMWHS Challenges*. Cham, Switzerland: Springer Cham; 2018, p. 190–98.
15. Baskaran L, Maliakal G, Al'Aref SJ, Singh G, Xu Z, Michalak K, et al. Identification and quantification of cardiovascular structures from CCTA: an end-to-end, rapid, pixel-wise, deep-learning method. *JACC Cardiovasc Imaging* 2020;13:1163–71.
16. Sharobeem S, Le Breton H, Lalys F, Lederlin M, Lagorce C, Bedossa M, et al. Validation of a whole heart segmentation from computed tomography imaging using a deep-learning approach. *J Cardiovasc Transl Res* 2022;15:427–37.
17. Chen HH, Liu CM, Chang SL, Chang PY, Chen WS, Pan YM, et al. Automated extraction of left atrial volumes from two-dimensional computer tomography images using a deep learning technique. *Int J Cardiol* 2020;316:272–8.
18. Abdulkareem M, Brahier MS, Zou F, Taylor A, Thomaides A, Bergquist PJ, et al. Generalizable framework for atrial volume estimation for cardiac CT images using deep learning with quality control assessment. *Front Cardiovasc Med* 2022;9:822269.
19. Mahabadi AA, Balcer B, Dykun I, Forsting M, Schlosser T, Heusch G, et al. Cardiac computed tomography-derived epicardial fat volume and attenuation independently distinguish patients with and without myocardial infarction. *PLoS One* 2017;12:e0183514.
20. Milanese G, Silva M, Bruno L, Goldoni M, Benedetti G, Rossi E, et al. Quantification of epicardial fat with cardiac CT angiography and association with cardiovascular risk factors in symptomatic patients: from the ALTER-BIO (Alternative Cardiovascular Bio-Imaging markers) registry. *Diagn Interv Radiol* 2019;25:35–41.
21. Masuda M, Mizuno H, Enchi Y, Minamiguchi H, Konishi S, Ohtani T, et al. Abundant epicardial adipose tissue surrounding the left atrium predicts early rather than late recurrence of atrial fibrillation after catheter ablation. *J Interv Card Electrophysiol* 2015;44:31–7.
22. Hoori A, Hu T, Lee J, Al-Kindi S, Rajagopalan S, Wilson DL. Deep learning segmentation and quantification method for assessing epicardial adipose tissue in CT calcium score scans. *Sci Rep* 2022;12:2276.
23. Siriapisith T, Kusakunniran W, Haddawy P. A 3D deep learning approach to epicardial fat segmentation in non-contrast and post-contrast cardiac CT images. *PeerJ Comput Sci* 2021;7:e806.
24. Lu CF, Hsu FT, Hsieh KL, Kao YJ, Cheng SJ, Hsu JB, et al. Machine learning-based radiomics for molecular subtyping of gliomas. *Clin Cancer Res* 2018;24:4429–36.
25. Bartoli A, Fournel J, Ait-Yahia L, Cadour F, Tradi F, Ghattas B, et al. Automatic deep-learning segmentation of epicardial adipose tissue from low-dose chest CT and prognosis impact on COVID-19. *Cells* 2022;11:1034.
26. Nalepa J, Marcinkiewicz M, Kawulok M. Data augmentation for brain-tumor segmentation: a review. *Front Comput Neurosci* 2019;13:83.
27. Sacks HS, Fain JN. Human epicardial adipose tissue: a review. *Am Heart J* 2007;153:907–17.
28. Franssens BT, Nathoe HM, Leiner T, van der Graaf Y, Visseren FL; SMART Study Group. Relation between cardiovascular disease risk factors and epicardial adipose tissue density on cardiac computed tomography in patients at high risk of cardiovascular events. *Eur J Prev Cardiol* 2017;24:660–70.
29. Liu Z, Wang S, Wang Y, Zhou N, Shu J, Stamm C, et al. Association of epicardial adipose tissue attenuation with coronary atherosclerosis in patients with a high risk of coronary artery disease. *Atherosclerosis* 2019;284:230–6.
30. Wang TD, Lee WJ, Shih FY, Huang CH, Chang YC, Chen WJ, et al. Relations of epicardial adipose tissue measured by multidetector computed tomography to components of the metabolic syndrome are region-specific and independent of anthropometric indexes and intraabdominal visceral fat. *J Clin Endocrinol Metab* 2009;94:662–9.
31. Taha AA, Hanbury A. Metrics for evaluating 3D medical image segmentation: analysis, selection, and tool. *BMC Med Imaging* 2015;15:29.
32. Commandeur F, Goeller M, Razipour A, Cadet S, Hell MM, Kwiecinski J, et al. Fully automated CT quantification of epicardial adipose tissue by deep learning: a multicenter study. *Radiol Artif Intell* 2019;1:e190045.
33. He X, Guo BJ, Lei Y, Wang T, Fu Y, Curran WJ, et al. Automatic segmentation and quantification of epicardial adipose tissue from coronary computed tomography angiography. *Phys Med Biol* 2020;65:095012.